Inorganic Chemistry

Communication

pubs.acs.org/IC

Addition of a Second Binding Site Increases the Dynamic Range but Alters the Cellular Localization of a Red Fluorescent Probe for Mobile Zinc

Andrei Loas,[‡] Robert J. Radford,[‡] and Stephen J. Lippard*[,‡]

[‡]Department of Chemistry, Massachusetts Institute of Technology, Cambridge, Massachusetts 02139, United States

Supporting Information

ABSTRACT: We report the synthesis and photophysical properties of ZBR4 and ZR1, two resorufin-based ditopic probes for mobile zinc. Upon binding Zn^{2+}, the sensors display 14- and 41-fold enhancements of their red fluorescence emission, respectively. In contrast to ZR1 and other members of the ZBR family, which accumulate in the endoplasmic reticulum, ZBR4 spontaneously localizes to the mitochondria of HeLa cells. The modular approach in designing the constructs facilitates a homologation strategy aimed at tuning the zinc-binding and intracellular targeting properties of future probes.

Zinc is a key element for life.[1] Although most intracellular Zn^{2+} ions are tightly bound to metalloproteins, mobile forms are found throughout the cell.[2] Of particular interest is the role of zinc in neurobiology. Select neurons accumulate large amounts of mobile Zn^{2+} in presynaptic vesicles. Vesicular zinc is released upon stimulation, modulating protein function and regulating synaptic plasticity.[3] Dysregulation of zinc homeostasis in the brain is associated with epilepsy, Alzheimer's disease, and excitotoxicity.[4] Appropriate tools for the detection and quantification of mobile zinc at discrete cellular locales are critical for understanding its biology.[5] Fluorescence imaging with small-molecule probes has emerged as the biologically non-intrusive method of choice for in vivo visualization.[6]

Although a large collection of fluorescent sensors for Zn^{2+} are available,[5−7] organelle-specific probes with low ($\lambda \geq 600$ nm) excitation and emission energies remain an identified need. Recently, we developed the ZBR family of benzoresorufin-based analogues, containing a single $[N_3O]$ metal-binding motif. The red ZBR sensors are bright and show adventitious localization to the endoplasmic reticulum (ER);[8] their synthesis, however, is cumbersome, and the fluorescence enhancement upon binding Zn^{2+} is only moderate. Building on knowledge gained in designing green fluorescein-based probes,[9−11] we sought to expand the range of available red derivatives with constructs containing two $[N_3O]$ units. Owing to photoinduced electron transfer from two zinc-binding amine moieties, ditopic sensors are expected to display a more efficient fluorescence quenching in the metal-free form, as previously reported for the QZ2[10] and ZPP1[11] probes. Derivatization of the fluorophore with electron-withdrawing groups should further improve the dynamic range through a decrease in the amine pK_a values and minimization of proton-induced emission turn-on.[7] On the basis of these principles and using the 2,2′-dipicolylamine (DPA) motif, we designed ZBR4 and ZR1, the first ditopic resorufin-based sensors for mobile Zn^{2+} (Scheme 1).

Scheme 1. Synthesis of ZBR4 and ZR1, Highlighting in Red the Atoms of the $[N_3O]$ Metal-Binding Sites[a]

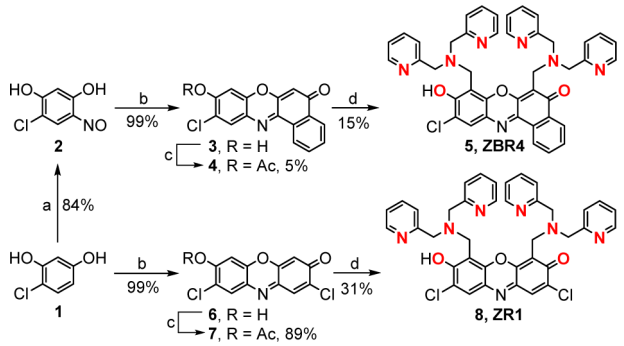

[a]Conditions: (a) *i*-amyl nitrite, KOH, EtOH, 25 °C; (b) 1,3-dihydroxynaphthalene or **2**, concentrated H_2SO_4, 110 °C; (c) acetic anhydride, Py, reflux; (d) DPA, paraformaldehyde, MeCN, reflux.

To prepare the new probes, we employed the modular approach initially devised for phenoxazone derivatives.[12,13] To impart selectivity for a single ditopic product, 10-chloro-9-hydroxybenzoxazone [chlorobenzoresorufin (**3**); Scheme 1] was synthesized through acid-catalyzed condensation of 4-chloro-6-nitrosoresorcinol (**2**)[14] with 1,3-dihydroxynaphthalene. The remarkably low solubility of **3** precluded an efficient direct conversion to the desired sensor and returned only a 5% yield of the acetylated analogue (**4**). Compound **4**, however, was completely soluble under the Mannich reaction conditions and provided the ditopic probe ZBR4 (**5**, Scheme 1) in 15% isolated yield. Applying a similar strategy, we appended two DPA binding sites to the previously unexplored 2,8-dichloro-7-hydroxyphenoxazone[14] fluorophore [dichlororesorufin (**6**)], affording the symmetric ZR1 analogue, **8**, in 31% yield. See Figures S1−S16 for characterization.

With ZBR4 and ZR1 in hand, their photophysical properties were investigated (Table S2). In the metal-free form, ZBR4 displays a broad absorption band with a maximum at ∼570 nm at pH 7. Discrete changes were observed in its visible spectrum upon binding of the first (blue shift, Figure S17A) and second

Received: March 31, 2014
Published: June 10, 2014

   dx.doi.org/10.1021/ic500732z | *Inorg. Chem.* 2014, 53, 6491−6493

(red shift, Figure S17B) equivalents of Zn^{2+}, respectively. The absorption maximum in the Zn^{2+}-saturated form occurs at 573 nm. Both the metal-free and Zn^{2+}-bound species of ZBR4 emit in the red region at ~630 nm (Figures 1A and S19), translating into

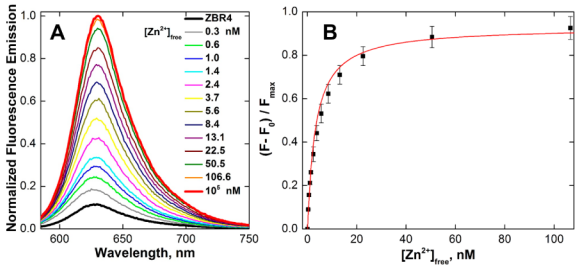

Figure 1. Normalized (A) fluorescence emission spectra and (B) integrated fluorescence response of 1 μM ZBR4 vs free Zn^{2+} concentrations in aqueous buffer containing 1 mM EGTA ($ZnSO_4$, 25 °C, 100 mM KCl, 50 mM PIPES, pH 7.0, λ_{ex} = 560 nm).

an ~60 nm Stokes shift. ZR1, in contrast, exhibits an orange Zn^{2+}-bound emission maximum at 611 nm and only an 18 nm Stokes shift (Figures S18 and S19).

Both sensors manifest a large enhancement of fluorescence emission upon Zn^{2+} binding. Average 14- and 41-fold increases in the resorufin-standardized[15] fluorescence quantum yields (Φ) were observed when excess Zn^{2+} was added to buffered aqueous solutions of ZBR4 and ZR1, respectively (Figure S19 and Table S2). The associated brightness values ($\varepsilon\Phi$) increased, on average, 18- and 44-fold to 1.84 and 2.43 × 10^4 M^{-1} cm^{-1}, respectively. Compared with the maximal increase in brightness of ~8-fold among the monotopic ZBR sensors,[8] addition of a second DPA unit in ZBR4 more than doubled the dynamic range.

The ZBR4 probe displayed nanomolar binding affinity for mobile zinc. The apparent Zn^{2+} dissociation constant ($K_{d,app}$) was determined by fluorescence titration in aqueous buffer containing 1 mM (ethylene glycol)bis(2-aminoethyl ether)-*N*,*N*,*N*′,*N*′-tetraacetic acid (EGTA), a competing ligand allowing for $[Zn^{2+}]_{free}$ of up to 110 nM (Table S1). Saturation of both binding sites was confirmed by a <5% increase in fluorescence upon addition of 100 μM $[Zn^{2+}]_{free}$, in order to provide the maximal response (Figure 1). Fitting a nonlinear model[9] to the plot of the normalized fluorescence response vs $[Zn^{2+}]_{free}$ provided a $K_{d,app}$ value of 3.25 ± 0.12 nM.

In the case of Zn^{2+}-bound ZR1, a constant decrease in the fluorescence intensity was noticed during the titration experiments, precluding an accurate determination of $K_{d,app}$ (Figures S28 and S29). This observation prompted a more careful examination of the stability of ZBR4 and ZR1 in solution. Using the red absorption maxima of the chlorobenzoresorufin (ZBR4) and dichlororesorufin (ZR1) scaffolds as a spectroscopic handle, we determined that both metal-free sensors retained >95% stability in pH 7 aqueous buffer over 24 h at 25 °C (Figures S26A and S27A). Upon saturation with Zn^{2+}, however, the absorption bands associated with ZBR4 and ZR1 decreased by ~20% and ~50%, respectively, over 24 h (Figures S28 and S30). In contrast, both Zn^{2+}-bound sensors are stable in deionized water lacking a buffer (Figure S35). An HPLC−mass spectrometry analysis of concentrated solutions of both Zn^{2+}-bound and metal-free ZR1 indicated that the two major degradation products correspond to the loss of one and two picolyl moieties, respectively (Figure S36).

At 37 °C, when dissolved in cell-imaging medium (dye- and serum-free DMEM), the absorption band of ZBR4 decreased by ca. 30% over 3 h (Figure S26). Despite this apparent degradation of the sensor, addition of Zn^{2+} to this solution produced a >15-fold increase in fluorescence emission (Figure S31). Under similar conditions, ZR1, as well as the parent fluorophores **3** and **6**, remained ≥95% stable in medium (Figures S27B and S32). Taken together, the stability data suggest that, following attachment to the resorufin scaffolds, the DPA units of the two sensors become susceptible to chemical alterations, which are accelerated upon binding of Zn^{2+} and even in the presence of buffering agents.

We further explored the proton-binding properties of the two sensors. Variations in pH elicit substantial changes in the absorption and emission profiles of ZBR4 and ZR1 in solution (Figures S20 and S21). Plotting the normalized emission of metal-free ZBR4 vs pH revealed distinct protonation events. A nonlinear fit to these data (Figure S20B) produced three apparent pK_a values: pK_{a1} = 6.26 ± 0.05, pK_{a2} = 3.24 ± 0.14, and pK_{a3} = 2.14 ± 0.09. In the case of ZR1, only two values were obtained: pK_{a1} = 6.47 ± 0.1 and pK_{a2} = 1.37 ± 0.18 (Figure S21). We attribute the lowest pK_a values to protonation of the resorufin core.[15] Notably, the apparent pK_{a1} values <7 are advantageous for biological imaging because H^+-induced fluorescence turn-on is minimized for both sensors at physiological pH.

ZBR4 and ZR1 undergo a zinc-selective fluorescence response. Treatment of aqueous solutions of ZBR4 and ZR1 with alkali and alkaline-earth metals did not affect their fluorescence emission, whereas binding of paramagnetic first-row transition-metal ions caused fluorescence quenching (Figures S22 and S23). Addition of Zn^{2+} resulted in complete (for Na^+, Mg^{2+}, and Ca^{2+}) or partial (for Mn^{2+} and Fe^{2+}) restoration of the fluorescence.

The ability of the new ditopic probes to detect intracellular mobile Zn^{2+} was investigated in live HeLa cells. Both sensors are readily cell-permeable, and strong fluorescence signals can be obtained using short incubation times and low sensor concentrations in the incubation medium (Figure 2). An ~two-fold increase in the integrated intracellular fluorescence response was observed for both sensors following application of 50 μM exogenous Zn^{2+} as its 1:2 complex with pyrithione (ZnPT; Figures 2C−E and S24C−E). Subsequent treatment of the cells with 50 μM of the chelator *N*,*N*,*N*′,*N*′-tetrakis(2-

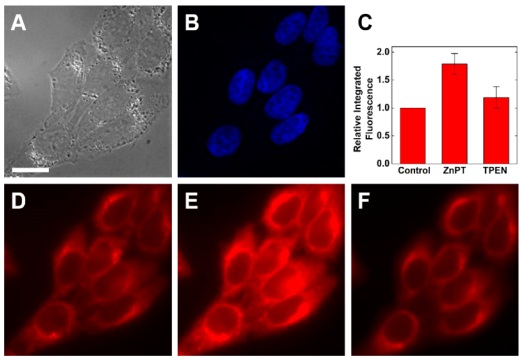

Figure 2. Fluorescence microscopy of live HeLa cells incubated with 1 μM ZBR4 and 10 μM Hoechst 33258 at 37 °C for 15 min. (A) Differential interference contrast (DIC) image. (B) Nuclear staining by Hoechst 33258. (C) Quantification of Zn^{2+}-induced fluorescence response (mean ± SD; *N* = 54). ZBR4 signal (D) before addition of exogenous Zn^{2+}, (E) 5 min after treatment with 50 μM ZnPT, and (F) 5 min after addition of 50 μM TPEN. Scale bar = 15 μm.

dx.doi.org/10.1021/ic500732z | *Inorg. Chem.* 2014, 53, 6491−6493

pyridylmethyl)ethylenediamine (TPEN) largely reversed the fluorescence signal (Figures 2F and S24F). Addition of TPEN to cells untreated with ZnPT did not produce a significant change in fluorescence (not shown).

The foregoing results demonstrate the applicability of ZBR4 and ZR1 for imaging intracellular mobile Zn^{2+}. The fluorescence response observed in a live cell environment, however, was substantially lower than expected based on cuvette studies. The high background fluorescence of the two sensors could be explained by partial protonation occurring within the cell or upon accumulation at specific locales.

The intracellular localization of ZBR4 and ZR1 was also investigated. Coincubation of HeLa cells with ZBR4 and organelle-specific markers Hoechst 33258 and ER-Tracker Blue-White (Figures 2 and 3E) indicated that the sensor does

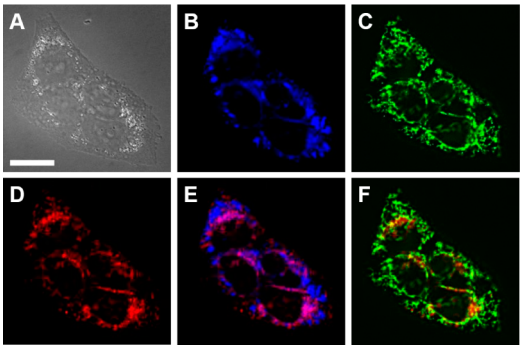

Figure 3. Colocalization analysis of ZBR4 with organelle-specific markers in live HeLa cells incubated with 1 μM ZBR4, 2 μM ER-Tracker Blue-White DPX, and 0.5 μM MitoTracker Green FM at 37 °C for 15 min. (A) DIC image. (B) ER-Tracker Blue-White DPX. (C) MitoTracker Green. (D) ZBR4. (E) Overlay of ZBR4 and ER-Tracker. (F) Overlay of ZBR4 and MitoTracker Green. Scale bar = 15 μm.

not localize strongly[16] to either the nucleus or the ER (Pearson's correlation coefficients,[17] r, of −0.2 and 0.33, respectively). A strong correlation ($r = 0.66 \pm 0.08$; $N = 82$) was obtained in the overlap with MitoTracker Green (Figure 3F), however, indicating accumulation of ZBR4 within the mitochondria. This finding makes ZBR4 a valuable addition to the limited selection of red-emitting mitochondrial probes for Zn^{2+}.[5,18] Its altered cellular localization is intriguing because ZBR4 is the only member of the ZBR family that fails to accumulate in the ER,[8] despite sharing a similar benzoresorufin scaffold. In contrast, ZR1 localizes strongly to the ER, judging by the r value of 0.63 ± 0.07 ($N = 50$) obtained in the overlap with ER-Tracker (Figure S25). Furthermore, ZR1, ZBR4, and ZP1[9] all share the ditopic, DPA-based zinc-binding motif but localize to the ER, mitochondria, and Golgi apparati, respectively. The parent fluorophores **3** and **6**, as well as the acetylated analogue **7**, were cell-impermeable under similar incubation conditions. There was minimal permeation and a visual overlap with ER-Tracker Green in the case of **4** (Figures S33 and S34). These observations emphasize the difficulty in designing small-molecule, organelle-specific fluorescent sensors in a predictable manner and highlight the importance of the pendant zinc-binding units in imparting cellular permeability to resorufin-based probes.

Clearly, our knowledge regarding the mechanism by which molecular probes accumulate at discrete subcellular sites remains incomplete. Given the tight homeostatic regulation of mobile zinc levels in the cell, the ability to develop organelle-targetable, small-molecule fluorescent constructs becomes critically important. To this end, the synthetic strategy employed in the design of the ditopic ZBR4 and ZR1 sensors offers distinct advantages toward facile structural modifications of both the fluorophore and the Zn^{2+}-binding motifs. An envisioned homologous series will help address the stability issues in solution, tune the photophysical and zinc-binding properties, and, at the same time, advance understanding of the factors determining spontaneous localization in live cells.

■ ASSOCIATED CONTENT

Ⓢ Supporting Information

Experimental details, NMR and HRMS data, analytical HPLC traces, absorption, emission and pH profiles, metal selectivity, fluorescence microscopy images, and stability studies. This material is available free of charge via the Internet at http://pubs.acs.org.

■ AUTHOR INFORMATION

Corresponding Author

*E-mail: lippard@mit.edu.

Notes

The authors declare no competing financial interest.

■ ACKNOWLEDGMENTS

This work was supported by NIH Grant GM065519 from the National Institute of General Medical Sciences. Instrumentation in the MIT DCIF is funded by Grant 1S10RR13886-01.

■ REFERENCES

(1) Maret, W. *Adv. Nutr.* **2013**, *4*, 82−91.
(2) Maret, W. *Met. Ions Life Sci.* **2013**, *12*, 479−501.
(3) Pan, E.; Zhang, X. A.; Huang, Z.; Krezel, A.; Zhao, M.; Tinberg, C. E.; Lippard, S. J.; McNamara, J. O. *Neuron* **2011**, *71*, 1116−1126.
(4) Frederickson, C. J.; Koh, J.-Y.; Bush, A. I. *Nat. Rev. Neurosci.* **2005**, *6*, 449−462.
(5) Dean, K. M.; Qin, Y.; Palmer, A. E. *Biochim. Biophys. Acta* **2012**, *1823*, 1406−1415.
(6) Que, E. L.; Domaille, D. W.; Chang, C. J. *Chem. Rev.* **2008**, *108*, 1517−1549.
(7) Nolan, E. M.; Lippard, S. J. *Acc. Chem. Res.* **2009**, *42*, 193−203.
(8) Lin, W.; Buccella, D.; Lippard, S. J. *J. Am. Chem. Soc.* **2013**, *135*, 13512−13520.
(9) Walkup, G. K.; Burdette, S. C.; Lippard, S. J.; Tsien, R. Y. *J. Am. Chem. Soc.* **2000**, *122*, 5644−5645.
(10) Nolan, E. M.; Jaworski, J.; Okamoto, K.-I.; Hayashi, Y.; Sheng, M.; Lippard, S. J. *J. Am. Chem. Soc.* **2005**, *127*, 16812−16823.
(11) Zhang, X.-a.; Hayes, D.; Smith, S. J.; Friedle, S.; Lippard, S. J. *J. Am. Chem. Soc.* **2008**, *130*, 15788−15789.
(12) Apfel, U. P.; Buccella, D.; Wilson, J. J.; Lippard, S. J. *Inorg. Chem.* **2013**, *52*, 3285−3294.
(13) Crossley, M. L.; Dreisbach, P. F.; Hofmann, C. M.; Parker, R. P. *J. Am. Chem. Soc.* **1952**, *74*, 573−578.
(14) Batchelor, R.; Ge, Y.; Gee, K.; Johnson, I.; Leung, W.-Y.; Liu, J.; Patch, B.; Smalley, P.; Steinberg, T. U.S. Patent 7,432,372, Oct 7, 2008.
(15) Bueno, C.; Villegas, M. L.; Bertolotti, S. G.; Previtali, C. M.; Neumann, M. G.; Encinas, M. V. *Photochem. Photobiol.* **2002**, *76*, 385−390.
(16) Zinchuk, V.; Wu, Y.; Grossenbacher-Zinchuk, O. *Sci. Rep.* **2013**, *3*, 1365.
(17) French, A. P.; Mills, S.; Swarup, R.; Bennett, M. J.; Pridmore, T. P. *Nat. Protoc.* **2008**, *3*, 619−628.
(18) Koide, Y.; Urano, Y.; Hanaoka, K.; Terai, T.; Nagano, T. *ACS Chem. Biol.* **2011**, *6*, 600−608.